J. Fluid Mech. (1990), *vol.* 220, *pp.* 539–567
Printed in Great Britain

The entrainment of bubbles by drop impacts

By HUGH C. PUMPHREY[1] AND PAUL A. ELMORE[2]
National Center for Physical Acoustics, PO Box 847, University, MS 38677, USA

(Received 15 January 1990)

Various processes are described by which a drop of water, impacting on a water surface, may entrain a bubble. There are: (i) irregular entrainment, in which the complex details of a splash entrain bubbles; (ii) regular entrainment, in which the crater formed by the drop impact develops in a predictable way to form a single bubble; (iii) entrainment of large bubbles, in which most of the volume of the crater is trapped as a bubble; and (iv) Mesler entrainment, in which many very small bubbles are trapped in the very early stages of the impact process; possibly between wave crests of capillary waves which develop on the drop and on the water surface. This last process is different from the preceding three in that it produces very little sound. All of the processes except the third one have been described individually in the literature; here we present them together for comparison. The regular entrainment process is discussed in the greatest detail and some new experimental results are presented which concern the size and nature of the entrained bubbles. The significance of the regular and irregular entrainment processes to the generation of underwater sound by rain is discussed.

1. Introduction

The various phenomena which occur when a drop of water strikes a water surface have been studied for many years (Worthington 1908); the crown-shaped splash which occurs immediately after the impact and the column of water which is then thrown upwards are well known. It is also well known (Franz 1959) that the sound produced by such drop impacts can be traced to two different mechanisms. These are, firstly, the 'water hammer' effect, in which a sharp pulse of sound is emitted when the drop first touches the surface, and secondly, the oscillation of bubbles which are entrained in the water by the flow which results from the impact. The bubble sound is a damped sinewave. The relative importance of these two effects in explaining the underwater sound of rain has been discussed in some detail in the literature (Nystuen 1986; Pumphrey & Crum 1990; Pumphrey, Crum & Bjørnø 1989). It has been a subject of debate because, although the bubble sound is louder, it does not occur for every drop. Franz could discover no pattern to its occurrence and therefore deemed it to be unimportant, but this conclusion was erroneous, as we shall show.

If we assume that both the drop and the surface are made of clean water, that the temperature is constant, the surface is horizontal and stationary and that the drop is spherical and falls vertically, there are only two parameters left for us to control: they are the drop diameter, d, and its impact velocity, v. In this paper we shall

[1] Present address: Cambridge University Engineering Department, Trumpington Street, Cambridge CB2 1PZ
[2] Present address: Millsaps College, Jackson, Mississippi, USA

describe the type of behaviour which occurs over as much of the (d, v)-plane as is possible. We shall see that the type of bubble entrainment described by Franz is but one of several distinct behaviours which may occur.

2. Experimental methods

Drops of water were produced by allowing water to flow slowly through glass tubes or hypodermic needles of various sizes; this works well for drops with diameters greater than 2 mm. Smaller drops are held too firmly by surface tension to even the smallest needle, so some alternative method was required. The most effective solution was to attach the hypodermic needle to the cone of a loudspeaker and then to vibrate the cone with a square wave of large amplitude; the apparatus is sketched in figure 1. Since the flow rate through the needle remains more or less constant, the drop size can be varied by changing the frequency of oscillation; the amplitude is adjusted to ensure that one drop detaches for each cycle of the square wave. The apparatus imparts a certain amount of horizontal velocity to the drops, but this velocity can usually be made small, again by adjusting the amplitude of vibration.

The impact velocity, v_I, of the drops was controlled by varying the height of fall, z, and was calculated (Pumphrey 1989) from the equation

$$v_I = v_T\left[1-\exp\left(\frac{-2gz}{v_T^2}\right)\right]^{\frac{1}{2}}, \tag{1}$$

where g is the acceleration due to gravity. The terminal velocity v_T was calculated from the drop diameter by a polynomial fit (Dingle & Lee 1972) to a set of experimental data (Gunn & Kinzer 1949). Equation (1) is calculated by assuming a constant drag coefficient, i.e. that the drag force on the drop is proportional to the square of the velocity; this assumption may be only approximately valid, but the resulting equation agrees well with the only set of published data available (Laws 1941).

In all studies the sound was detected with a miniature hydrophone (B&K 8103) and amplified by a conditioning charge amplifier (B&K 2635). From there, the signal was usually passed to a digital oscilloscope (LeCroy 9400) which was capable of capturing transient signals, calculating fast Fourier transforms and averaging them to give a power spectrum and performing various other signal processing tasks. The oscilloscope was interfaced via a GPIB bus to a computer (DEC MINC-73) which did additional signal processing. Many of the signals studied were damped sinusoids emitted by oscillating bubbles and the computer was used to make repetitive measurements of the frequencies and damping constants of these signals. Most of the studies were made in a large tank of water, approximately 1 m × 1 m × 1 m in size. The tank was not anechoic, but it was large enough that the signals reflected from the walls were not a great problem, especially at higher frequencies. The hydrophone was usually placed vertically below the splash at a depth of 50–100 mm, but could be placed anywhere in the tank, if required.

The sound-producing processes were also studied by high-speed cinematography. The camera used was a Photec IV and was usually run at a speed of 1000 or 2000 frames per second. The drop impact was photographed against a brightly lit background and the view was usually horizontal through the glass wall of the tank. In addition to photographing the impact an oscilloscope trace was recorded on the film, providing a simultaneous record of the behaviour of the water and the sound which it was producing; see Pumphrey *et al.* (1989) for further details.

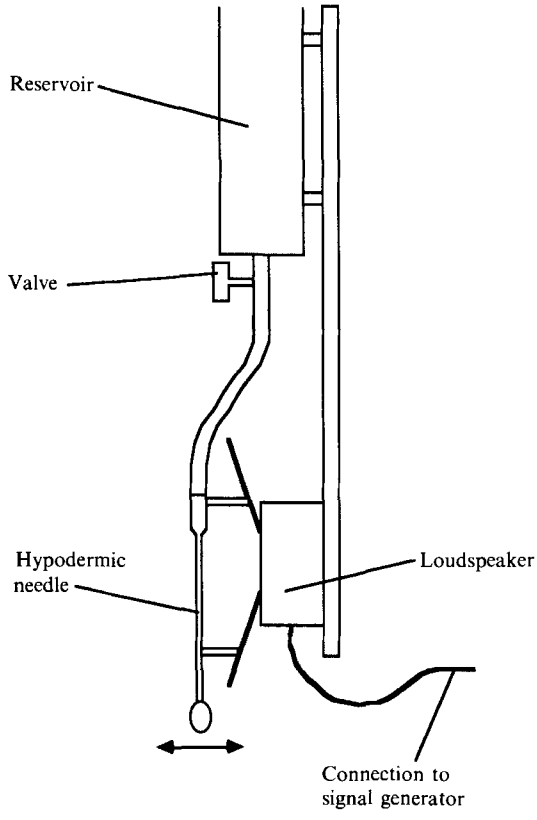

FIGURE 1. Sketch of the apparatus used to produce small drops. The loudspeaker is driven by a square-wave signal and shakes the hypodermic needle in the horizontal direction.

3. Irregular (Franz-type) entrainment

We have named the process described by Franz *irregular entrainment* because, given the drop diameter and impact velocity, one cannot predict whether a bubble will be entrained or not. Figure 2 shows a sequence of frames from a high-speed film of the irregular entrainment process. In frames (*g*) and (*l*), we can see distortions in the surface which are almost bubbles; in frames (*h*) and (*m*) these 'proto-bubbles' have detached from the surface and begun to oscillate. The one in frame (*h*) is entrained by the impact of a small satellite drop or 'Plateau's spherule', which detached from the needle at the same time as the main drop; the satellite drop can be seen in frame (*f*). The bubble in frame (*m*) is entrained by the collapse of the column of water seen in frames (*i–k*). For further examples, see Franz (1959) and Pumphrey *et al.* (1989). The important features to note here are that the entrainment of bubbles depends on the exact time of arrival of the Plateau's spherule and the details of the way the column collapses. These features vary enough from one drop to the next to make the process essentially unpredictable and unrepeatable, even for drops of nominally the same size and velocity. Even if one or more bubbles are entrained, their sizes (and hence their resonance frequencies) are very variable, as is the intensity of the sound emitted. The frequency may be as low as 500 Hz and as high as 100 kHz. One further phenomenon occurs at extremely high impact velocities: the 'crown' which is thrown up by the impact rises almost vertically and

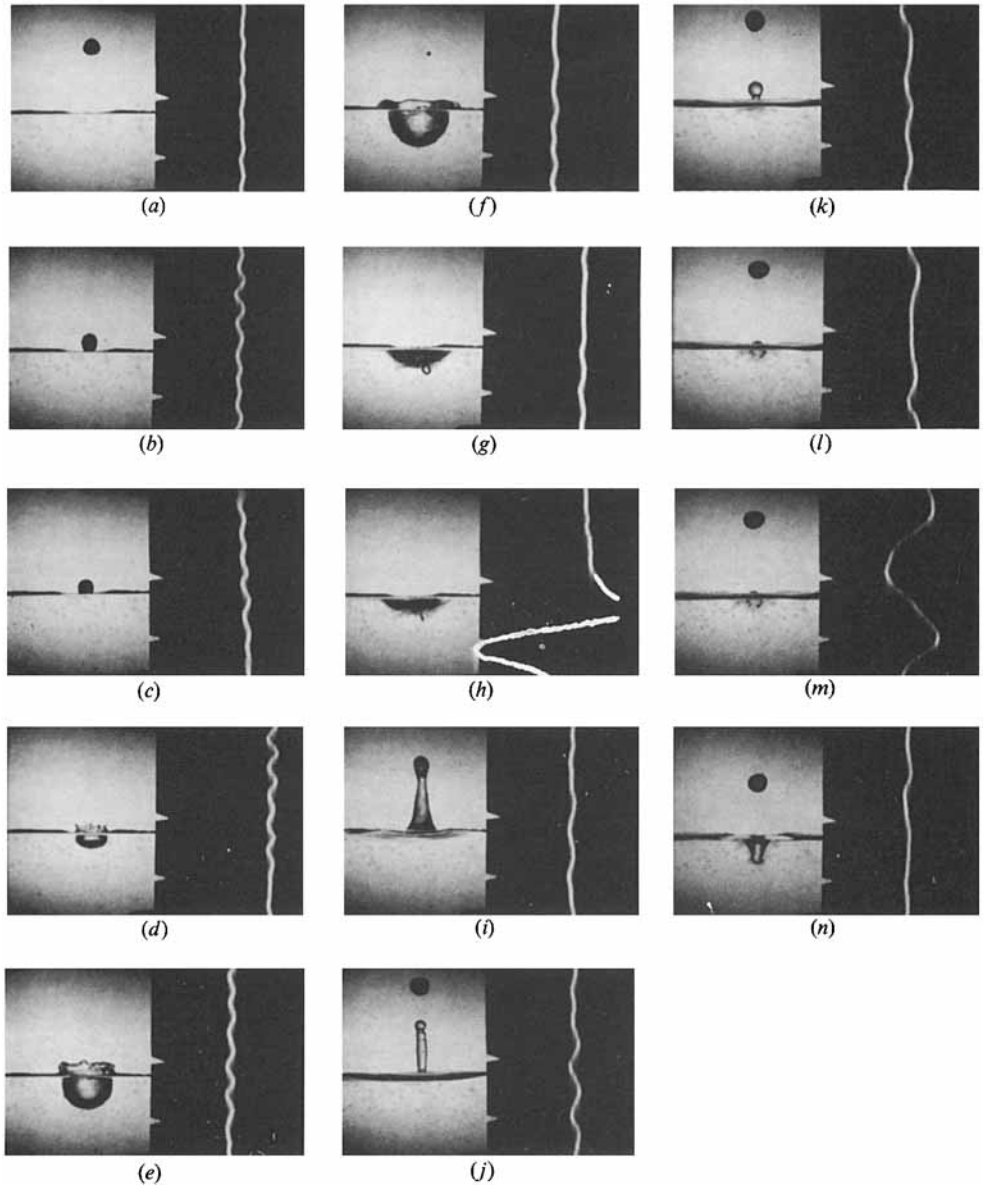

FIGURE 2. This is a sequence of frames from a high-speed movie of the irregular entrainment process caused by a drop of 5.8 mm in diameter impacting at a speed of 2.4 m/s. The original movie was taken at a speed of 4000 frames/s but these frames originate from the beginning of the film where it was still accelerating. The frames are in the correct order, of course, but are not necessarily consecutive, e.g. there were many frames on the original film between frames (*h*) and (*i*), which are not shown in the figure. The white line on a dark background to the right of each picture is an oscilloscope trace showing the acoustic pressure at the time the frame was taken. Times in ms after the initial impact for each frame are: (*a*) −9, (*b*) −0.5, (*c*) 0, (*d*) 4, (*e*) 14, (*f*) 30, (*g*) 46, (*h*) 49, (*i*) 90, (*j*) 127, (*k*) 148, (*l*) 159, (*m*) 159.3, (*n*) 177. Note that (*l*) and (*m*) are consecutive frames; the film had accelerated to about 3000 frames/s at this point. The bubble in frame (*h*) had a measured diameter of 1.2 ± 0.2 mm and a frequency of 5.4 ± 0.3 kHz; Minnaert's equation gives a frequency of 5.5 ± 1 kHz for this bubble size. For the bubble in frame (*m*) the values are similar. (From Pumphrey 1989).

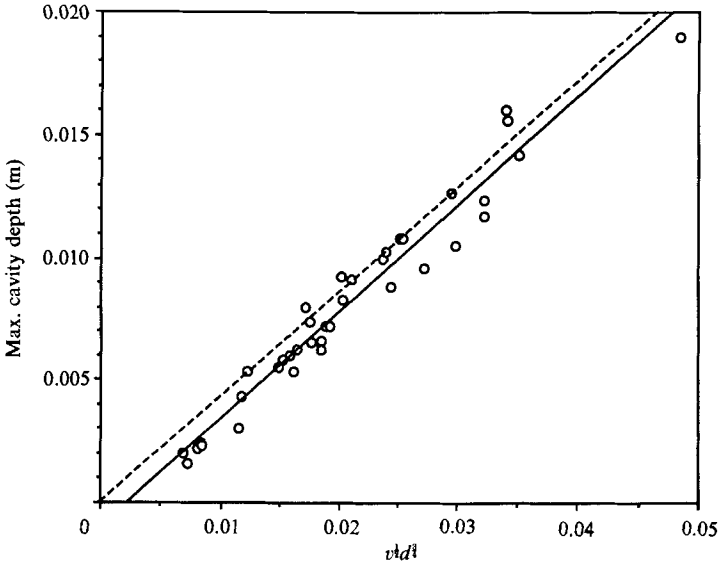

FIGURE 3. This graph shows how the maximum cavity depth varies with drop diameter and impact velocity. The dashed line is the theoretical result described in the text while the solid line is a best fit straight line to the data points. Their slopes are 0.44 (experimental) and 0.4293 (theoretical). The data were taken from high-speed movies; the experimental error is about ± 1 mm. (From Pumphrey 1989).

joins together at the top to form a very large bubble floating at the surface (Franz 1959; Engel 1966).

The fluid dynamics of the splash are rather complex, but one feature which we may describe with simple theory is the maximum depth, $R_{\max}$, of the cavity or crater seen in frames (*e*) and (*f*) of figure 2 (A. Prosperetti 1989, private communication). As that figure shows, the crater is approximately hemispherical; it is therefore simple to calculate its gravitational potential energy, E_p. We can then equate this to the kinetic energy, E_k, of the impacting drop. We assume that the cavity has no kinetic energy when at its maximum depth because the water has stopped flowing outwards and is about to start flowing in. Surface tension is neglected; for large splashes it is a small correction, while for small ones the theory breaks down anyway because the cavity ceases to be hemispherical. E_k is given by

$$E_k = \tfrac{1}{2}mv^2 = \tfrac{1}{12}\pi\rho d^3 v^2 \tag{2}$$

where ρ is the density of water and m is the drop's mass. E_p is given by $E_p = Mgz$, where M is the mass of the displaced hemisphere of water, and z is the depth of its centre of gravity. Since z is given by $z = \frac{3}{8}R_{\max}$, and M is given by $M = \frac{2}{3}\pi\rho R_{\max}^3$ we can show that

$$E_p = \tfrac{1}{4}\pi R_{\max}^4 \rho g. \tag{3}$$

Equating (2) and (3) gives

$$\tfrac{1}{3}d^3v^2 = gR_{\max}^4, \tag{4}$$

and hence

$$R_{\max} = (\tfrac{1}{3}g)^{\frac{1}{4}} d^{\frac{3}{4}} v^{\frac{1}{2}}. \tag{5}$$

If we plot $R_{\max}$ against $d^{\frac{3}{4}}v^{\frac{1}{2}}$ we should get a straight line of slope $(1/3g)^{\frac{1}{4}}$. As figure 3 shows, the agreement is remarkably good, even for rather small energies, at which surface tension distorts the spherical shape of the cavity. The experimental values are in general a little below the theoretical result; this is probably because some of

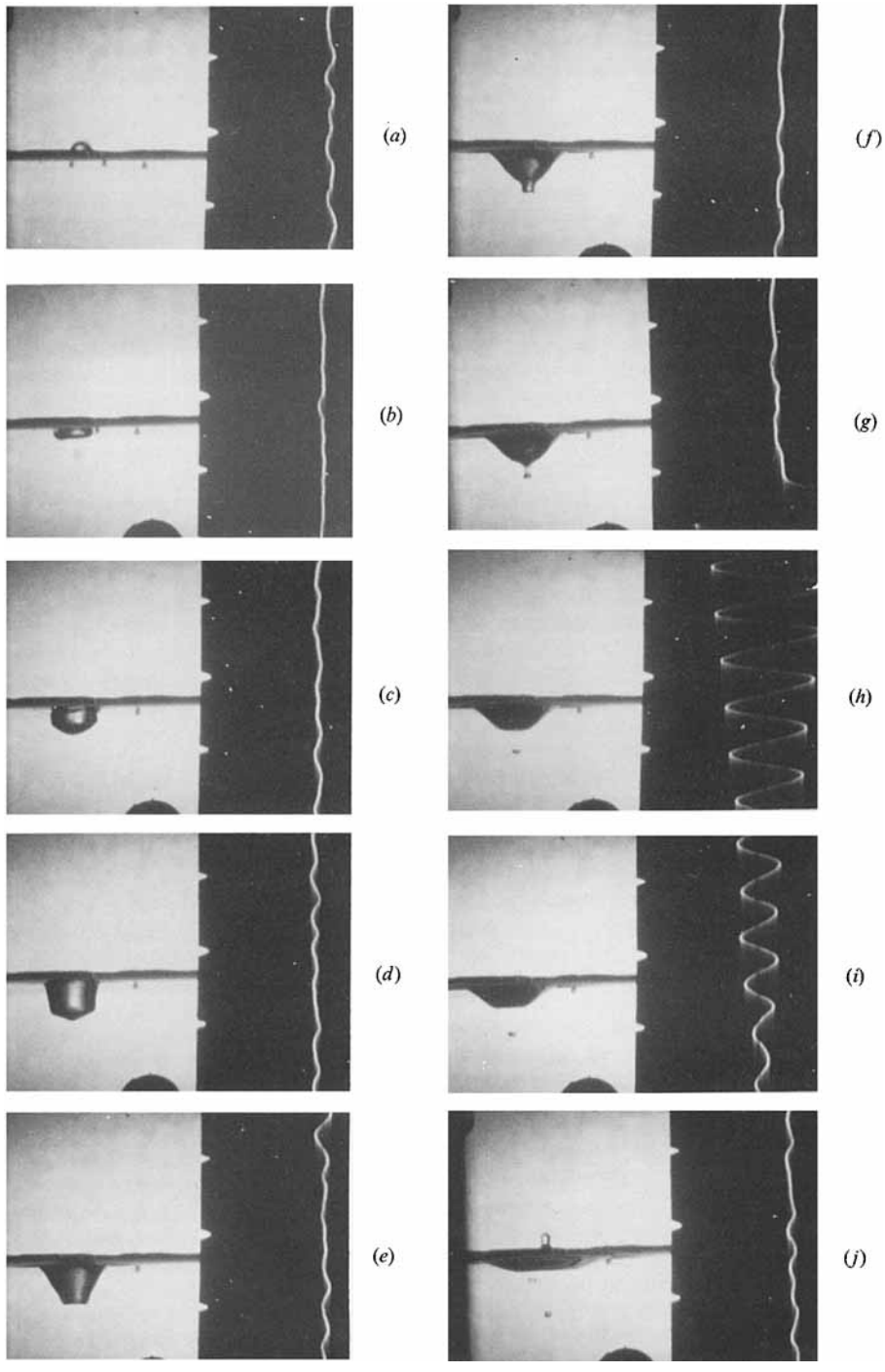

FIGURE 4. Frames from a high-speed movie showing regular entrainment as caused by a drop of 3.2 mm diameter impacting at 1.5 m/s. As in figure 2, the frames are in order but are not necessarily consecutive. The black object at the lower edge of the picture is the hydrophone. The line down the right-hand side of each frame is an oscilloscope trace showing the acoustic pressure; note the damped sinusoidal oscillation caused by the bubble in frames (*g–i*). The camera was

the kinetic energy of the drop does not go into potential energy of the cavity, but into the crown (see Engel 1966). Also, we have assumed that the flow velocity is instantaneously zero everywhere when the cavity is at maximum depth. It is not possible to describe other features of the splash, such as the time between the impact and the cavity reaching its maximum depth, with the sort of simple arguments outlined above; it is necessary to use computer simulation (Nystuen 1986; Harlow & Shannon 1967). Even this is of little or no use in predicting whether a bubble will be entrained.

4. Regular entrainment

As one goes to smaller drops and lower impact velocities, bubble entrainment as described by Franz becomes less and less frequent. However, one eventually reaches a region in which a different sort of entrainment occurs. It is different because it is predictable, a bubble will be formed by every drop within a certain range of drop diameters and impact velocities. Even the size of the bubble and the amplitude of the acoustic wave emitted are more or less predictable. This process was first described by Pumphrey & Walton (1988) but it was not realised at that time that it was fundamentally different from that discovered by Franz. Figure 4 shows frames from a high-speed cinematographic film of the process. Note that the bubble seems to be formed by the interplay of gravitational and surface tension effects; it does not require the presence of a Plateau's spherule or the collapse of a water column which are characteristic of irregular entrainment. The precise region over which the process occurs is shown in figure 5; note that it includes drops which impact at their terminal velocity. We shall use this fact later, to explain the generation of underwater sound by rain.

4.1. *Regular entrainment: why it occurs*

It is not fully understood at present why regular entrainment occurs, or why it occurs only within a small region of the (d, v)-plane. Gravity and surface tension are the two most important forces acting, so it would seem useful to re-plot the boundaries of the regular entrainment in terms of the Froude number, Fr, and the Weber number, We, defined by

$$Fr = \frac{v^2}{dg} \tag{6}$$

and

$$We = \frac{\rho v^2 d}{\sigma}, \tag{7}$$

where ρ is the density and σ the surface tension of the water. The results are shown in figure 6. The boundaries are approximately straight lines if one plots Fr on a logarithmic scale and We on a linear one, which suggests that they may be represented by expressions of the form

$$Fr = A\,\mathrm{e}^{B\,We}. \tag{8}$$

running at 950 frames/s so one frame is slightly greater than 1 ms. Times in ms (correct to 0.5 ms) after the initial impact for each frame are as follows: (*a*) 0, (*b*) 3.0, (*c*) 6.5, (*d*) 11.5, (*e*) 17.0, (*f*) 19.0, (*g*) 20.0, (*h*) 21.0, (*i*) 22.0, (*j*) 31.5. The entrained bubble had a measured diameter of 0.89 ± 0.08 mm and a frequency of 6.5 ± 0.2 kHz; Minnaert's equation gives a frequency of 7.4 ± 0.6 kHz for this bubble size.

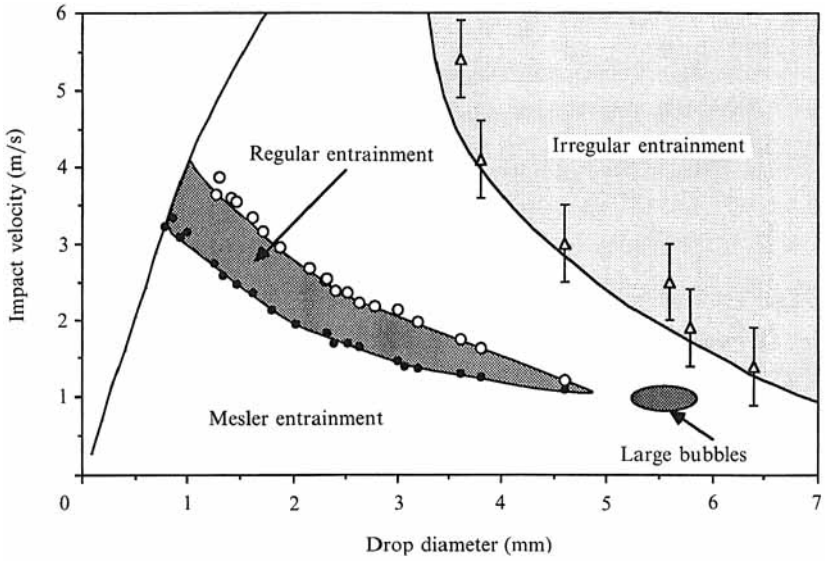

FIGURE 5. A plot showing the ranges of drop diameter d and impact velocity v for which various sorts of entrainment occur. The data points shown are the experimental values used to draw the shaded regions. The curve to the left of the figure is the terminal velocity curve.

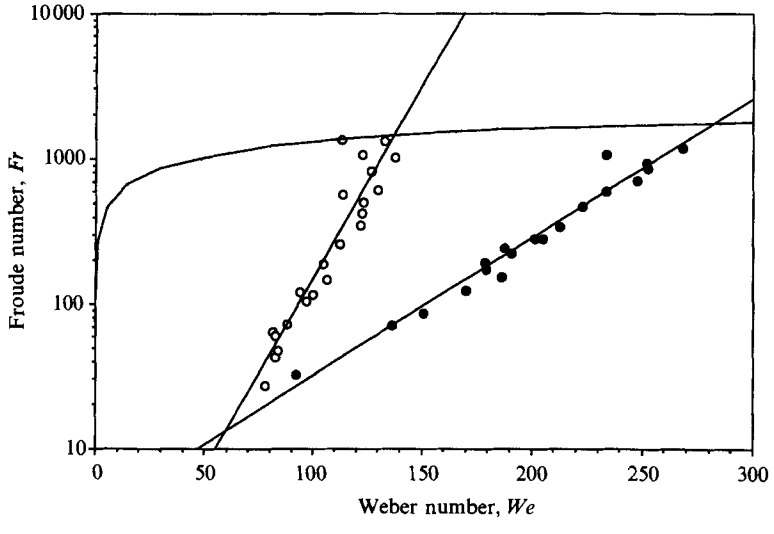

FIGURE 6. The boundaries of the regular entrainment region, plotted in terms of the Froude and Weber numbers. The filled circles correspond to the highest velocity that causes entrainment, the open circles to the lowest velocity. The line with no data points is the terminal velocity curve.

Here, A and B are dimensionless constants; there would be a different A, B pair for the upper and lower boundary. This is thought-provoking, but unfortunately does not provide much help in understanding how the process works. It would be very useful to know if the same effect occurred for other liquids and if the boundaries fell at the same values of We and Fr. It has been shown (Pumphrey *et al.* 1989) that the addition of a surfactant to the water can prevent the regular entrainment process

occurring at all, but the surfactant has a more complicated effect than to simply lower the surface tension because of the time taken for the surface film to spread over newly formed surfaces (Rayleigh 1890).

The development of the crater, as seen in the high-speed films, suggests a possible mechanism which might be the cause of regular entrainment. This mechanism consists of a capillary wave, which travels down the sides of the crater (Pumphrey 1989). When this wave reaches the bottom of the crater, its crest closes in from all sides, thus trapping the bubble. This is a speculative idea; attempts to use it to calculate when entrainment should occur have had only limited success. An alternative description (Oguz & Prosperetti 1990*a*) is that 'Whether a bubble is entrapped or not is determined by a delicate balance between the times at which the outward motion of the crater walls is reversed at different positions'. This statement probably contains a greater element of truth than the capillary wave idea, but is even less use in constructing a simple theory to predict when a bubble will be formed. A further possibility is that the process is somehow related to the way in which the drop changes shape as it falls; this is known to be important in determining whether an impacting drop forms a vortex ring (Chapman & Critchlow 1967). It seems that the only way to make progress towards a theoretical description of regular entrainment is to investigate the problem using numerical analysis.

Early computer simulations of drop impacts (Nystuen 1986; Harlow & Shannon 1967) do not show regular entrainment either because they omit surface tension or because they describe impacts in the wrong range of drop sizes and velocities. Once regular entrainment was discovered experimentally, a deliberate attempt was made to simulate it numerically (Oguz & Prosperetti 1990*a*). It was found that the calculation was unstable because the surface-tension terms caused spurious ripples to appear on the surface; fortunately it proved possible to suppress these by numerically smoothing the surface. When this was done the computer reproduced to a reasonable degree of accuracy the form of the surface deformations, the parameter range over which entrainment occurs and the time between impact and entrainment. Some typical results are shown in figure 7, others can be found in Oguz & Prosperetti (1990*a*, *b*) and Longuet-Higgins (1990).

Numerical simulation allows us to make predictions about when regular entrainment will occur and what size of bubble will be produced. It is less useful in giving us any physical insight into why it occurs and does not really help us to decide which (if either) of the capillary wave idea or the 'time of reversal of motion' idea is the most meaningful. It does, however, show that shape oscillations of the drop are not significant, because it succeeds in simulating the process beginning with a spherical drop.

4.2. *Regular entrainment: the sound emitted*

The sound emitted by the bubble is a damped sinewave as can be seen in figure 4. Since the bubble is a simple acoustic source which is very close to a pressure release boundary, the far-field sound pressure is given by:

$$p = \frac{D}{r} e^{-\beta(t-r/c)} \cos\theta \, e^{i(\omega t - kr)}, \tag{9}$$

where θ is the polar angle (measured from the downwards vertical), r is the distance from the bubble and t is time. As usual, β is a damping constant, ω is the angular resonance frequency, k is the wavenumber and c is the speed of sound. The initial dipole strength, D, is dependent on a number of factors, such as the depth of the

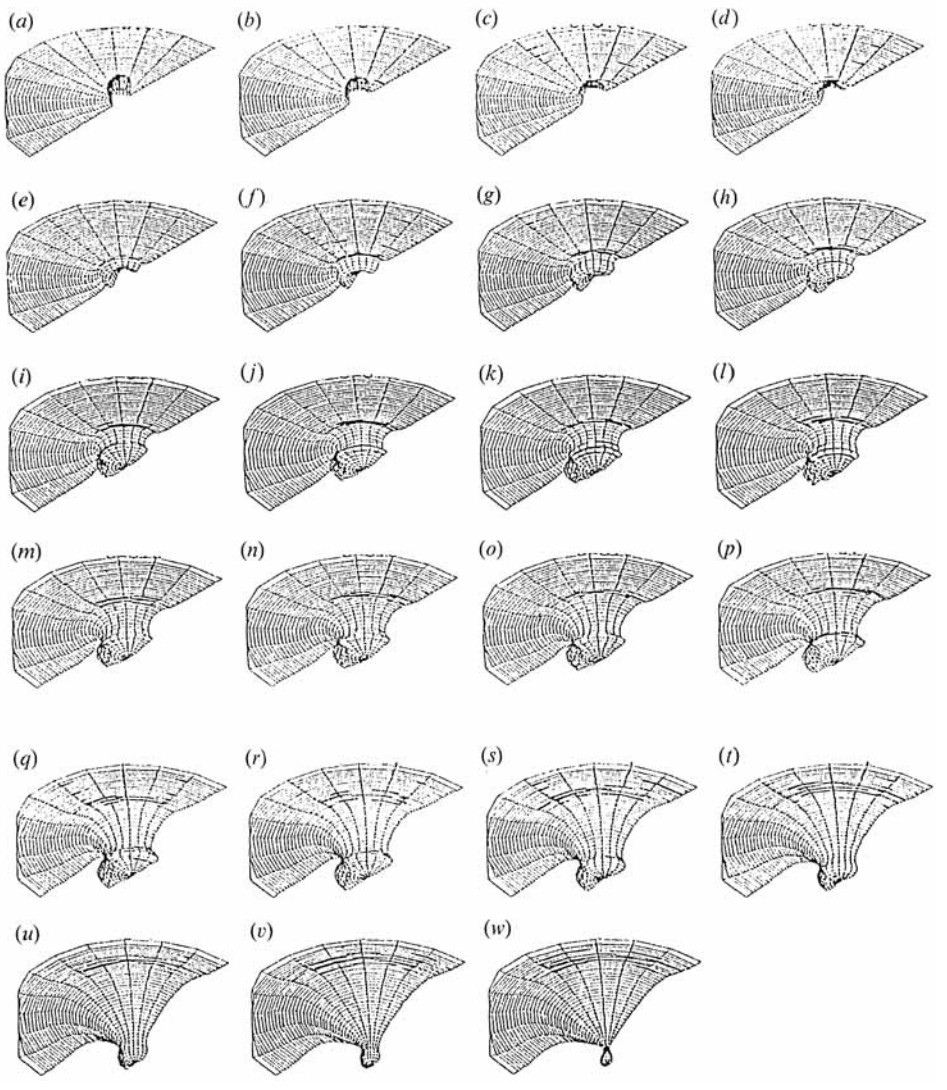

FIGURE 7. Computer simulation of regular entrainment. The surface shown represents the water surface; the time t after the moment of impact in dimensionless units (in this case, one dimensionless unit is approximately 1 ms) is (*a*) $t = 0$, (*b*) 0.241, (*c*) 0.572, (*d*) 0.919, (*e*) 1.293, (*f*) 1.739, (*g*) 2.238, (*h*) 2.774, (*i*) 3.422, (*j*) 3.913, (*k*) 4.320, (*l*) 4.807, (*m*) 5.664, (*n*) 6.869, (*o*) 8.084, (*p*) 9.063, (*q*) 10.577, (*r*) 12.602, (*s*) 14.970, (*t*) 17.472, (*u*) 19.723, (*v*) 21.576, (*w*) 22.723. (Figure by H. N. Oguz & A. Prosperetti, private communication.)

bubble below the surface. Most of the parameters in (9) may be measured experimentally and checked with theory; for example, the frequency is given by Minnaert's formula (Minnaert 1933):

$$\omega = \frac{1}{a_0}\left(\frac{3\gamma P_0}{\rho}\right)^{\frac{1}{2}}. \tag{10}$$

In this formula, P_0 is the static pressure in the water around the bubble, approximately equal to the atmospheric pressure, and γ is the ratio of specific heats

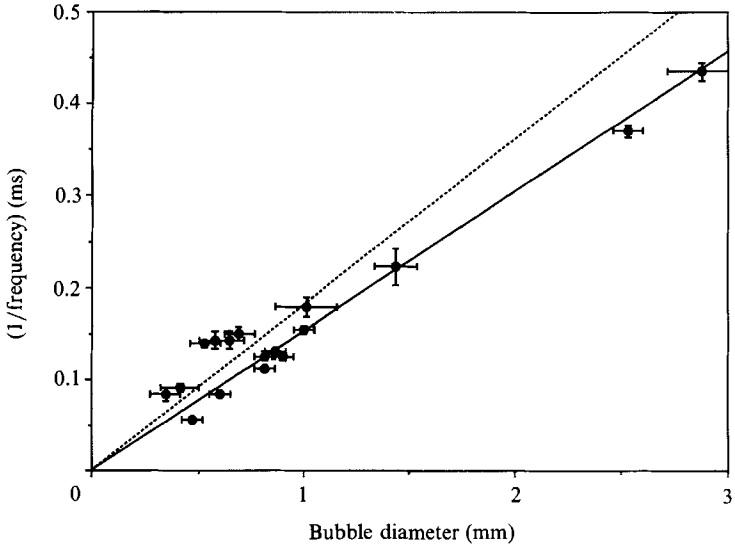

FIGURE 8. Minnaert's Equation. The data points are experimental results, taken from high-speed cinematographic films; the bars are rough estimates of the measurement error. The solid line is the locus of Minnaert's equation for a bubble containing gas with a ratio of specific heats, γ, of 1.4 as one would expect for a diatomic gas such as air. If the gas inside the bubble behaved isothermally, instead of adiabatically, then γ would be replaced by unity, this is shown by the dotted line. Bubbles oscillating at their resonance frequencies should all behave very nearly adiabatically, except at very high frequencies.

of the gas inside the bubble. This may be tested by comparing measured bubble diameters and oscillation frequencies from high-speed films; typical results are shown in figure 8. The errors are largely due to the difficulties involved in making measurements from films; when these are taken into account the agreement with theory is quite good. The damping constant, β, is much more difficult to calculate than the frequency. There are three different mechanisms by which a bubble may lose energy: they are viscous losses, which are important at very high frequencies, thermal losses which dominate between 1 kHz and 1 MHz, and losses due to acoustic radiation, which are most important at low frequencies (Devin 1959; Prosperetti 1988). The acoustic radiation damping is affected by the presence of the free surface; if we correct for this (Crowther 1988), we get reasonable agreement with theory, as shown in figure 9. Equation (9) suggests that we should be able to show experimentally that p is proportional to $1/r$ and to $\cos\theta$. This was done by recording the amplitude of the first cycle of bubble sound pulses at various points in the tank. Typical results are shown in figure 10, where acoustic pressure is plotted as a function of distance in various directions and as a function of angle at various distances. The pressure falls off as $1/r$ in all directions except horizontally; the polar plot of pressure against angle is roughly circular, as it should be.

The sound emitted by a regularly entrained bubble is more or less a damped sinusoid, as we have described, and as one would expect of a damped, undriven harmonic oscillator. The behaviour of the bubble after it has begun to oscillate is well understood, but it is less clear how it gets its initial energy. Longuet-Higgins (1990) has identified three possibilities, which are: (i) The Laplace pressure, i.e. the excess pressure inside the bubble due to surface tension after it has closed. (ii) The radial

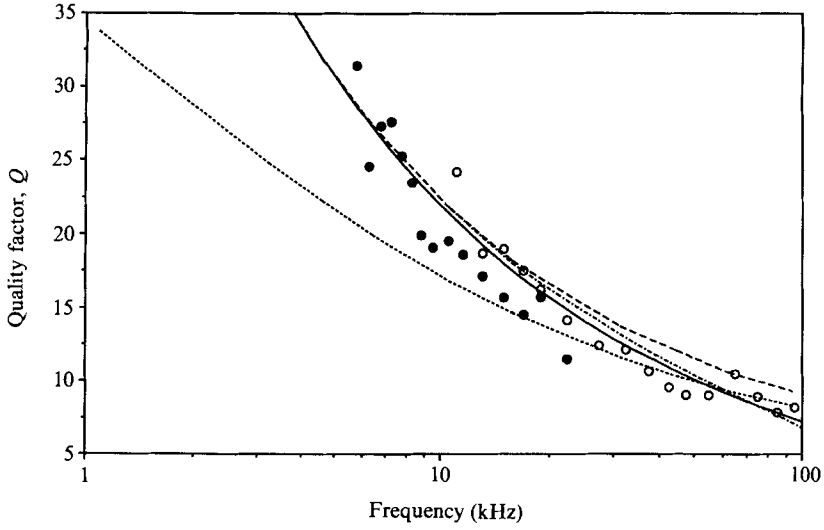

FIGURE 9. Quality factor $Q = \omega/2\beta$ as a function of frequency. The open circles are from bubbles entrained by a spray of small drops falling at terminal velocity, the filled circles represent bubbles regularly entrained by larger, slower drops. The dotted line is Prosperetti's theory, while the dashed line is the same theory with the acoustic damping δ_{ac} reduced to zero. The dot-dash line includes all three damping mechanisms, but with δ_{ac} corrected for the presence of the free surface (Crowther 1988). Finally, the solid line is a power-law fit to the data from the spray; it seems to agree best with the dot-dash line. This fit is used for calculations in a subsequent section. The random errors in the data are fairly small, approximately ± 1, and the various peaks, for example those at frequencies of 7, 10, and 60 kHz, are quite reproducible so they must be either systematic errors or a real physical effect.

motion of the water surrounding the bubble at the moment of closure. (iii) Surface oscillations on the bubble, which do not themselves radiate, but which can couple nonlinearly into the volume mode. The surface waves themselves might be caused by the non-spherical shape of the bubble at the moment it is formed, or by non-radial components of the flow after formation.

We might add to these a fourth, the hydrostatic pressure which is imposed on the bubble when it is formed. Only the Laplace and hydrostatic mechanisms are amenable to a straightforward calculation, which we now present. Consider a bubble, just before and just after entrainment, as shown in figure 11. After entrainment, the bubble is compressed to a new equilibrium radius, a_0, by the hydrostatic pressure $p_H = \rho g h$ and the Laplace pressure $p_L = 2\sigma/a_0$. The bubble then oscillates about this new radius, creating a pressure variation at its surface with an initial amplitude of

$$p_i(a_0) = p_L + p_H = \rho g h + 2\sigma/a_0. \tag{11}$$

In an infinite liquid, this would give a pressure field of

$$p_{inf}(r,t) = (1/r)(\rho g h a_0 + 2\sigma)\, e^{-\beta(t-r/c)} \cos(\omega t - kr), \tag{12}$$

but the presence of the free surface reduces this to

$$\begin{aligned}\rho(r,\theta,t) &= (1/r)(\rho g h a_0 + 2\sigma)\, e^{-\beta(t-r/c)}\, 2hk \cos\theta \cos(\omega t - kr) \\ &= (D/r)\, e^{-\beta(t-r/c)} \cos\theta \cos(\omega t - kr). \end{aligned} \tag{13}$$

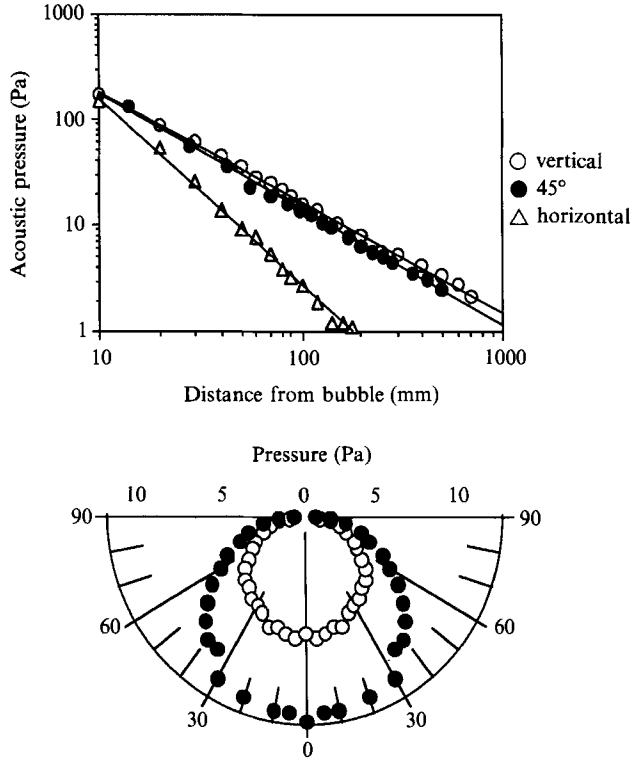

FIGURE 10. Radiation pattern of regularly entrained bubbles. The upper part of the figure is a plot of acoustic pressure against distance for three different directions; pressure is inversely proportional to distance in all directions except horizontally. The actual power laws given by a least-squares fit are vertical: 1.03, 45°: 1.09, horizontal: 1.76, with errors of less than 10%. The lower part is a plot of pressure against the polar angle at two different distances. Note that the pattern is circular, i.e. p is proportional to $\cos\theta$ as predicted. The bubbles had resonance frequencies of approximately 7–8 kHz.

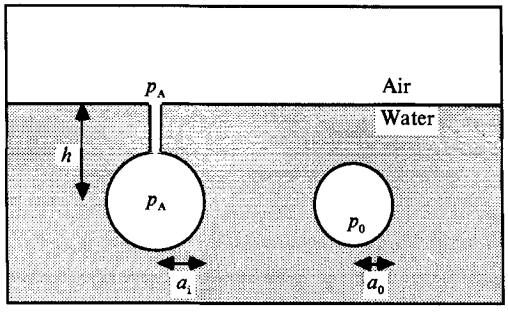

FIGURE 11. Sketch to show bubble before and after entrainment.

Hence, the initial dipole strength, D, is given by

$$D = 2hk(\rho g h a_0 + 2\sigma), \tag{14}$$

which, using Minnaert's formula (equation (10)) to substitute for a_0 gives

$$D(f) = (2gh^2/c)(3\gamma P_0 \rho)^{\frac{1}{2}} + (8\pi h\sigma/c)f. \tag{15}$$

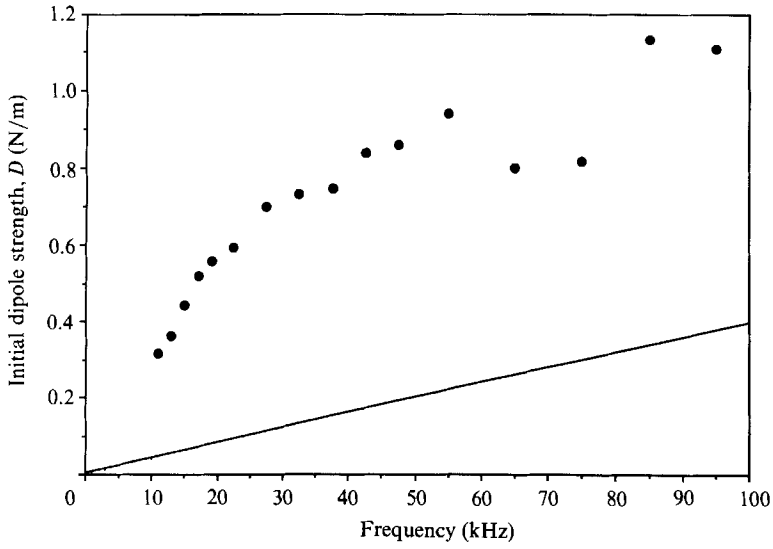

FIGURE 12. Initial dipole strength, D, as a function of resonance frequency for bubbles regularly entrained by a spray of small drops travelling at terminal velocity. The circles are experimental data; the straight line is the locus of equation (15).

We compare this with a set of data taken with a spray of small drops travelling at terminal velocity. High-speed films suggest that h is about 3.2 mm in this case, giving the result shown in figure 12. Note that the hydrostatic term is small compared to the surface-tension term. Even the Laplace pressure mechanism cannot account for all of the sound emitted; it predicts pressures of approximately 25 % of the experimental values. This suggests that at least one of the other possible mechanisms is dominant; we shall consider the surface wave mechanism next.

Close examination of high-speed film shows that bubbles are usually formed in rather aspherical shapes, and then undergo shape oscillations. These surface waves may persist for some 4–8 ms before the bubble settles down to a spherical shape. It has long been thought that the shape oscillations emit no sound (Strasberg 1956) but recent theoretical work (Longuet-Higgins 1989*a*, *b*) suggests that they might, in fact, be monopole sound sources. The idea is that by taking second-order terms in a perturbation expansion, it can be shown that the surface mode corresponding to the spherical harmonic of order n, which has a frequency of ω_n, can couple nonlinearly to the volume mode giving monopole radiation of sound with frequency $2\omega_n$. This effect will be particularly pronounced if $2\omega_n$ is approximately equal to ω, the resonance frequency of the volume mode, as given by (10). The calculations involved in this theory are very complicated. Longuet-Higgins has, however, estimated that for drop-entrained bubbles, surface waves can be no more important than the Laplace pressure.

The third possibility is that there is some radial flow in the water surrounding the bubble at the moment it is formed. If the proto-bubble becomes a free bubble at time $t = 0$ and has a radial wall velocity of U_0 at that time, the subsequent wall velocity oscillates sinusoidally with amplitude U_0. The dipole strength is given by

$$D = 2\rho c U_0 k^2 a_0^2 h, \tag{16}$$

so if we knew U_0, we could calculate D and compare it with measured values. There is no obvious theoretical way to find U_0; Longuet-Higgins (1990) has found an

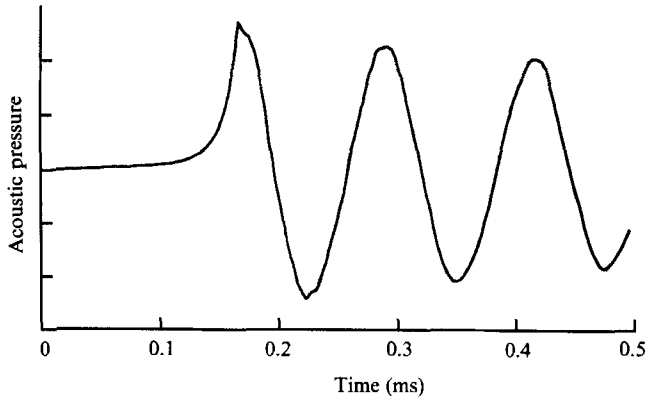

FIGURE 13. The beginning of a regular entrainment pulse; note that the pulse has the form of a damped sinusoid only after the first peak. The part before that peak, which is not part of a damped sinusoid, is shown on an expanded timescale in figure 13. The units of pressure are arbitrary, a typical peak pressure would be 0.7 Pa at a vertical distance of 1 m.

analytical approximation to the flow around the crater, which suggests that U_0 is, in fact, large enough to account for the observed D. Another possibility would be to obtain U_0 directly from a high-speed film, by making several measurements of the size of the proto-bubble during the time prior to its detachment. U_0 appears in the films to be negative, i.e. the bubble is contracting at the moment of detachment. Unfortunately, it has not so far been possible to obtain the magnitude of U_0 in this fashion because, at the frame rates used, the proto-bubble only appears in one or two frames of the film. Nevertheless, this last mechanism seems to be the most likely candidate.

Both the Laplace pressure and radial flow mechanisms suggest that the bubble is contracting at the moment it detaches. We can partially confirm this by examining the first cycle of a bubble oscillation in detail. Figure 13 shows a typical case; note that the pressure rises in a non-sinusoidal manner to the first peak, where damped sinusoidal oscillation begins. The pressure before that first peak can be adequately represented by an exponential increase (figure 14) so that the pressure at some point may be written as

$$p(r,\theta,\tau) = p_0(r,\theta)\,\mathrm{e}^{b\tau}, \qquad \tau < 0,$$

$$p_0(r,\theta)\,\mathrm{e}^{-\beta\tau}\cos\omega\tau, \quad \tau > 0, \tag{17}$$

where τ is the retarded time, $\tau = t - r/c$ and $p_0 = (D/r)\cos\theta$.

The acoustic pressure due to a spherical source with wall velocity $u(t)$, at a distance h below a free surface is given by

$$p(r,\theta,t) = \frac{2h\rho a^2\cos\theta}{rc}\,\ddot{u}(t-r/c), \tag{18}$$

where dots denote differentiation with respect to the argument. If p is given by (17), we can integrate it analytically three times, to find the acceleration, velocity and displacement of the bubble wall. The integration constants are dealt with by forcing the oscillatory part (i.e. the part where $\tau > 0$) to oscillate about zero and by making the functions continuous at $\tau = 0$. The damping constant, β, is small enough for us

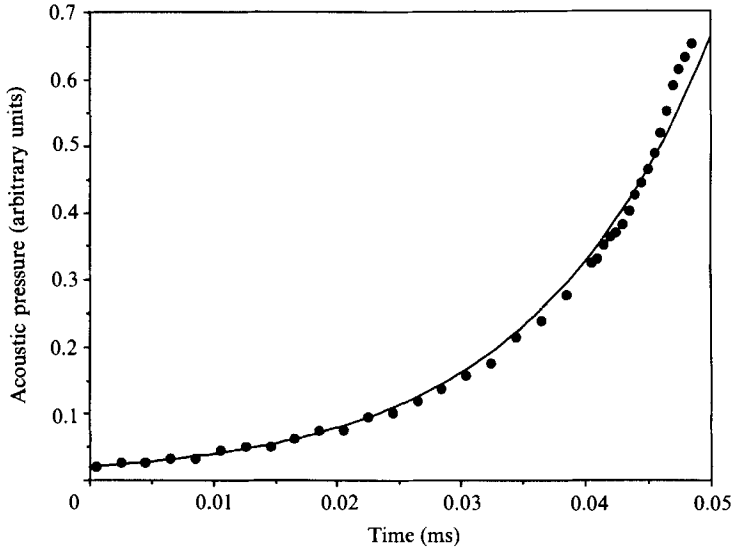

FIGURE 14. An expansion of the first quarter-cycle of figure 12. The circles are experimental data, while the curve is a best fit of the form $p = A\,e^{bt}$, where b is approximately $7.1 \times 10^4\ s^{-1}$.

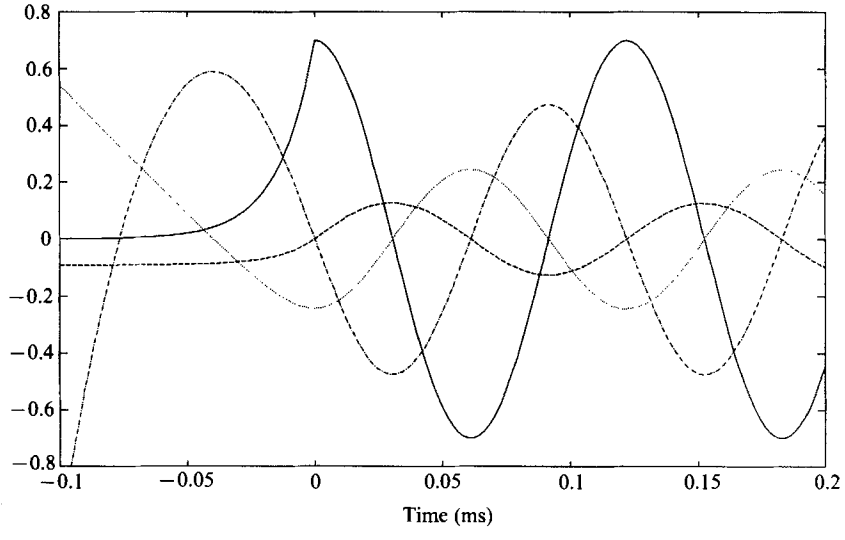

FIGURE 15. The motion of a bubble wall, as it is entrained. The curves are: solid line, acoustic pressure in Pascals; dashed line, bubble wall acceleration in units of $10^5\ m/s^2$, dotted line, wall velocity in m/s; dot-dash line, wall displacement in tens of μm. The pressure is given by (17), with $p_0 = 0.7\ N/m^2$ at a vertical distance of 1 m, and is plotted against retarded time $\tau = t - r/c$. The resonance frequency is 8.2 kHz, as in figures 12 and 13, giving a radius of 0.4 mm. The other curves are calculated from equations (19)–(21), taking $h = 5$ mm, $c = 1480$ m/s, $\rho = 1000\ kg/m^3$.

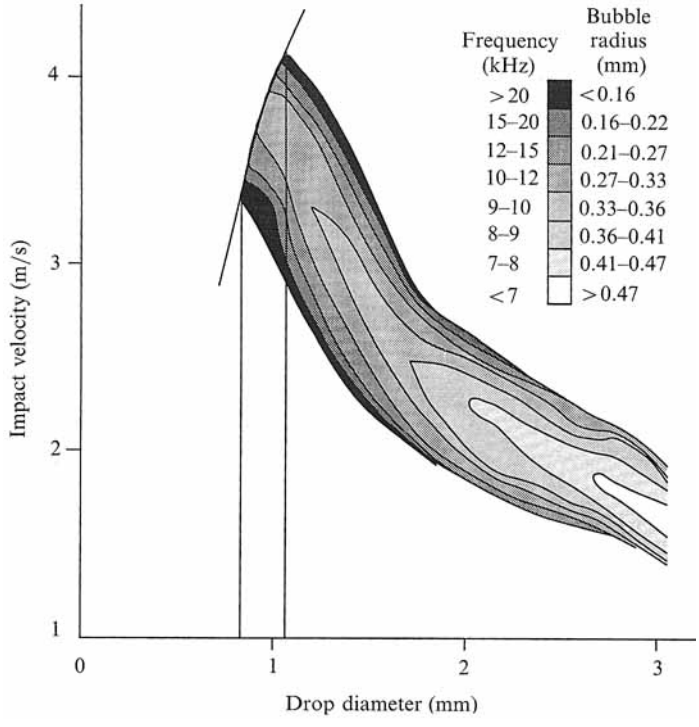

FIGURE 16. Contour plot showing how bubble size and resonance frequency vary with drop diameter and impact velocity for regularly entrained bubbles.

to ignore; its inclusion complicates the calculations a great deal without having a large effect on the result. We obtain

$$\frac{\mathrm{d}u}{\mathrm{d}\tau} = \frac{Dc}{2h\rho a^2}\frac{1}{b}(\mathrm{e}^{b\tau}-1), \qquad \tau < 0,$$

$$= \frac{Dc}{2h\rho a^2}\frac{1}{\omega}\sin\omega\tau, \qquad \tau > 0, \tag{19}$$

$$u = \frac{Dc}{2h\rho a^2}\left(\frac{1}{b^2}\mathrm{e}^{b\tau}-\frac{\tau}{b}-\frac{1}{\omega^2}-\frac{1}{b^2}\right), \qquad \tau < 0,$$

$$= \frac{-Dc}{2h\rho a^2}\frac{1}{\omega^2}\cos\omega\tau, \qquad \tau > 0,$$

$$x = \frac{Dc}{2h\rho a^2}\left(\frac{1}{b^3}\mathrm{e}^{b\tau}-\frac{\tau^2}{2b}-\left(\frac{1}{\omega^2}+\frac{1}{b^2}\right)\tau-\frac{1}{b^3}\right) \qquad \tau < 0, \tag{20}$$

$$= \frac{-Dc}{2h\rho a^2}\frac{1}{\omega^3}\sin\omega\tau, \qquad \tau > 0, \tag{21}$$

The results are plotted in figure 15; we can see that in the 50 μs prior to the time $t = 0$, the bubble is contracting as required. For times earlier than this, the curves are probably not meaningful, because the proto-bubble has not developed sufficiently for us to consider it as a spherical object separated from the surface. Note that the

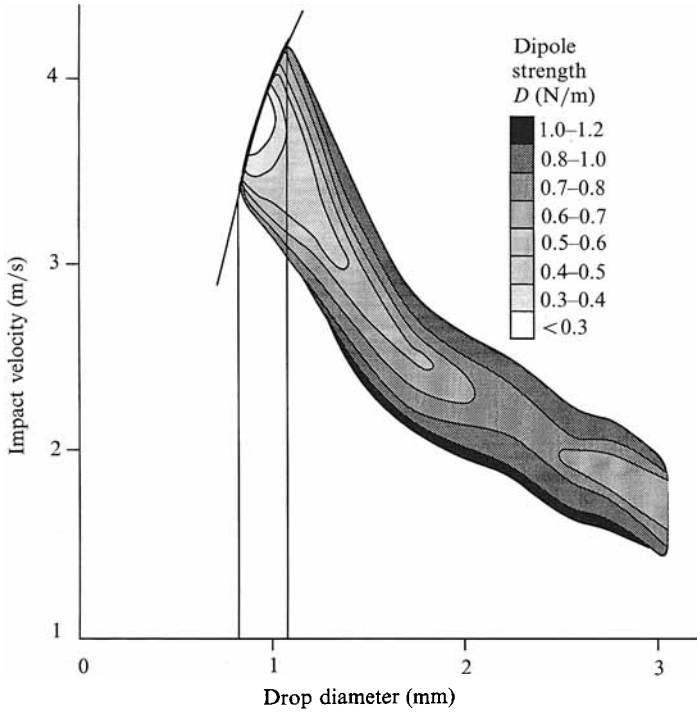

FIGURE 17. Contour plot showing how initial dipole strength varies with drop diameter and impact velocity for regularly entrained bubbles.

acceleration, velocity and displacement are all for a spherical bubble of the same volume as the real one. The real bubble is likely to be quite distorted, but this should not affect the sound radiated as the bubble is much smaller than a wavelength.

4.3. *Bubble sizes and dipole strengths*

We have investigated (Elmore, Pumphrey & Crum 1989) the details of the regular entrainment process, by recording dipole strengths and frequencies (and hence bubble sizes) over the entire range of drop sizes and impact velocities for which regular entrainment occurs. Some of the results are shown as contour plots in figures 16 and 17. These figures were constructed by extrapolating by hand between rather sparse data; accuracy is therefore limited approximately to the spacing between two adjacent contours. Nevertheless, they show the general features of the process quite nicely. Note that if one takes drops of a given size and slowly increases their impact velocity, both the frequency and the amplitude of the sound emitted first decrease and then increase again before entrainment ceases. If one decreases the drop size, adjusting the velocity so that the impact remains in the centre of the entrainment region, then the frequency increases, but the amplitude decreases. We were unable to produce drops which travelled faster than terminal velocity; the terminal velocity curve is shown in the upper left part of the figures. It can be seen from this that for drops travelling at terminal velocity, there is a small range of sizes for which regular entrainment will occur; this range is marked with two vertical lines on figures 16 and 17 and extends roughly from a diameter of 0.8 mm to one of 1.1 mm. This can be used to make some predictions about the bubbles that will be entrained by raindrops,

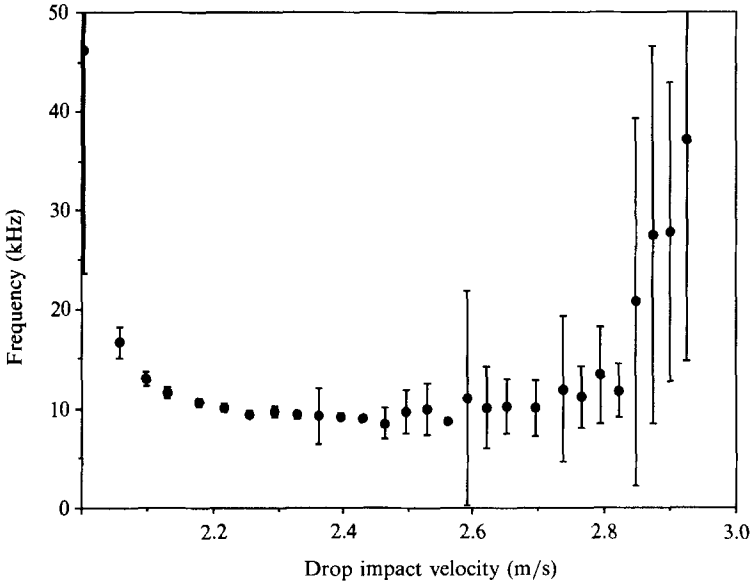

FIGURE 18. A typical sample of the data used to construct figure 16. The data are for a single drop diameter of 1.71 mm and show how the resonance frequency varies with impact velocity, in other words, it is a vertical section through figure 16. Each point is an average taken over 30 drop impacts; the bars are the standard deviation of the 30 values.

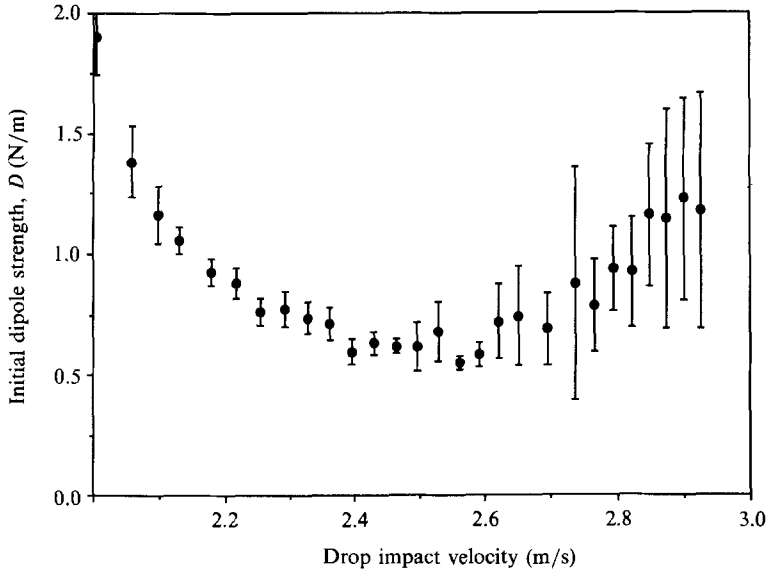

FIGURE 19. A typical sample of the data used to construct figure 17. Again, the data are for drops of 1.71 mm diameter; they show how the initial dipole strength, D, varies with impact velocity. Each point is an average taken over 30 drop impacts; the bars are the standard deviation of the 30 values.

which travel at terminal velocity. We can see from figure 16 that raindrops are not likely to entrain many bubbles with resonance frequencies below 12 kHz but that they will entrain bubbles with a wide range of higher frequencies, the highest coming from the edges of the entrainment region. Comparison with figure 17 shows that we

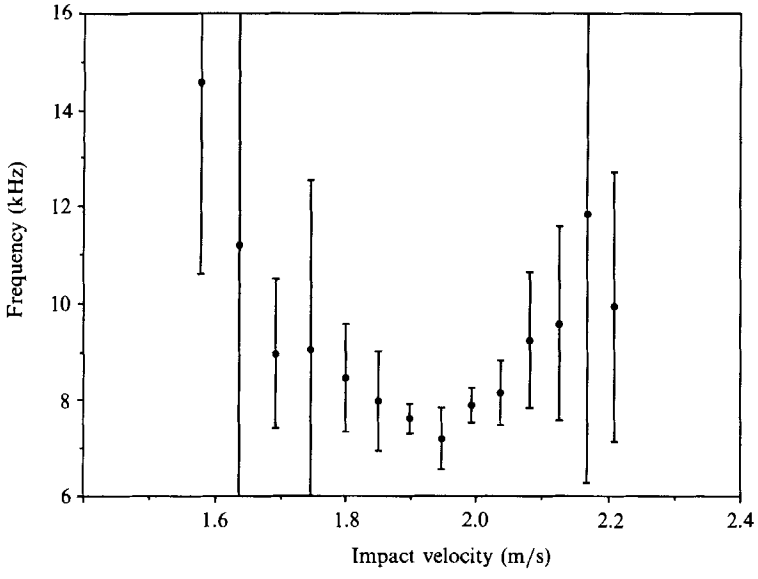

FIGURE 20. As figure 18, but for a single drop diameter of 2.57 mm.

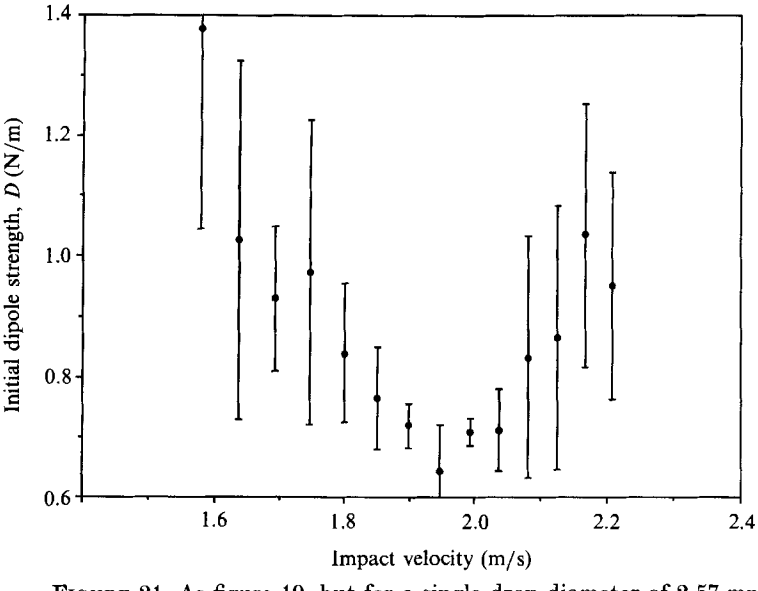

FIGURE 21. As figure 19, but for a single drop diameter of 2.57 mm.

should expect the 12 kHz bubbles to have dipole strengths of about 0.3 N/m and the 30 kHz bubbles to have dipole strengths of about 0.8 N/m. This agrees well with the results presented in figure 12.

Neither the frequency nor the dipole strength are exactly repeatable and they seem to be more variable at the edges of the entrainment region than in its centre. This is shown in figures 18–21, which show how both quantities, and their standard deviations, vary with impact velocity for drops of 1.71 mm and 2.57 mm in diameter.

The time between drop impact and bubble formation was also studied; the results are shown in figure 22. Note that the time increases with both drop size and with

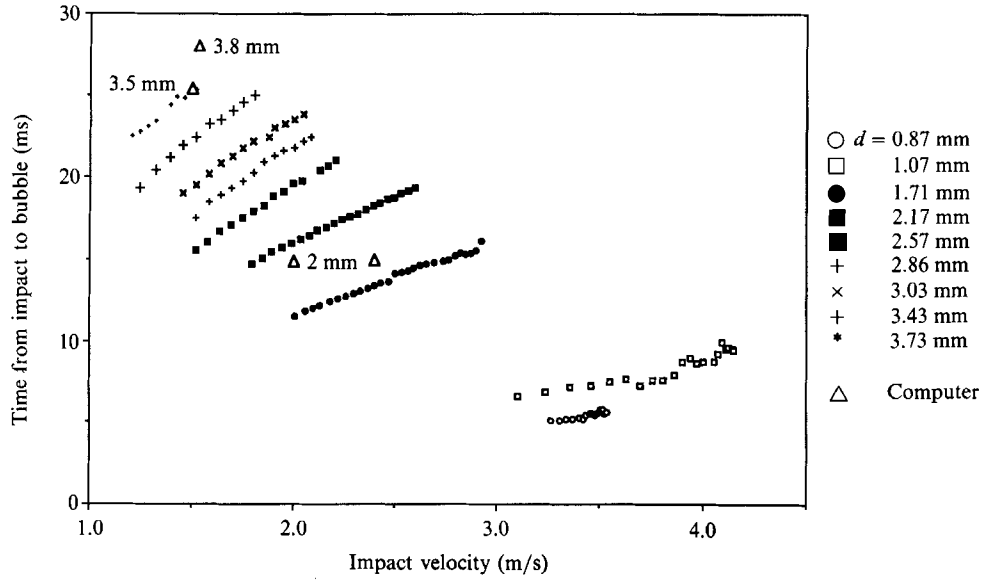

FIGURE 22. Plot of experimental values of the time between drop impact and bubble formation, as a function of impact velocity, for a range of drop sizes. Also, shown as triangles, are four times calculated by numerical simulation; they agree reasonably well with the experimental values. Note, however, that the times calculated for $d = 3.5$ and 3.8 mm are a little large, while the two times calculated for $d = 2$ mm do not show the expected increase of time with impact velocity.

impact velocity, also that the numerical results of Oguz & Prosperetti agree reasonably well with the experimental values.

5. Bubble entrainment and the sound of rain

The underwater noise of rain has been described in detail by Scrimger *et al.* (1987, 1989); the most obvious feature is a peak in the acoustic spectrum at a frequency of about 14 kHz, with a steep slope on the low-frequency side and a more gradual drop-off of 9 dB/octave on the high-frequency side. In this section, we describe some experiments which show that the peak is caused by regular entrainment of bubbles.

5.1. *Initial evidence*

The 14 kHz peak is easy to reproduce in the laboratory if one uses a spray of small drops falling onto a tank. It is important that the drops be small enough (0.7–1.2 mm in diameter is ideal) and that the spray be sparse enough so that each drop falls onto a fairly flat, undisturbed surface. The sound produced by such a spray consists of a series of damped sinusoids, like those produced by bubbles, and the averaged intensity spectrum closely resembles that of real rain. Further experimental evidence that the 14 kHz peak is in fact caused by bubbles is provided by the fact that the peak can be suppressed by the addition of surfactant to the water. It is known from experiments with individual drops that this prevents regular entrainment from occurring; figure 23 shows a typical high-speed film sequence from such an experiment. Figure 24 shows the acoustic power spectrum produced by a spray of small drops, before and after the addition of a surfactant in various concentrations.

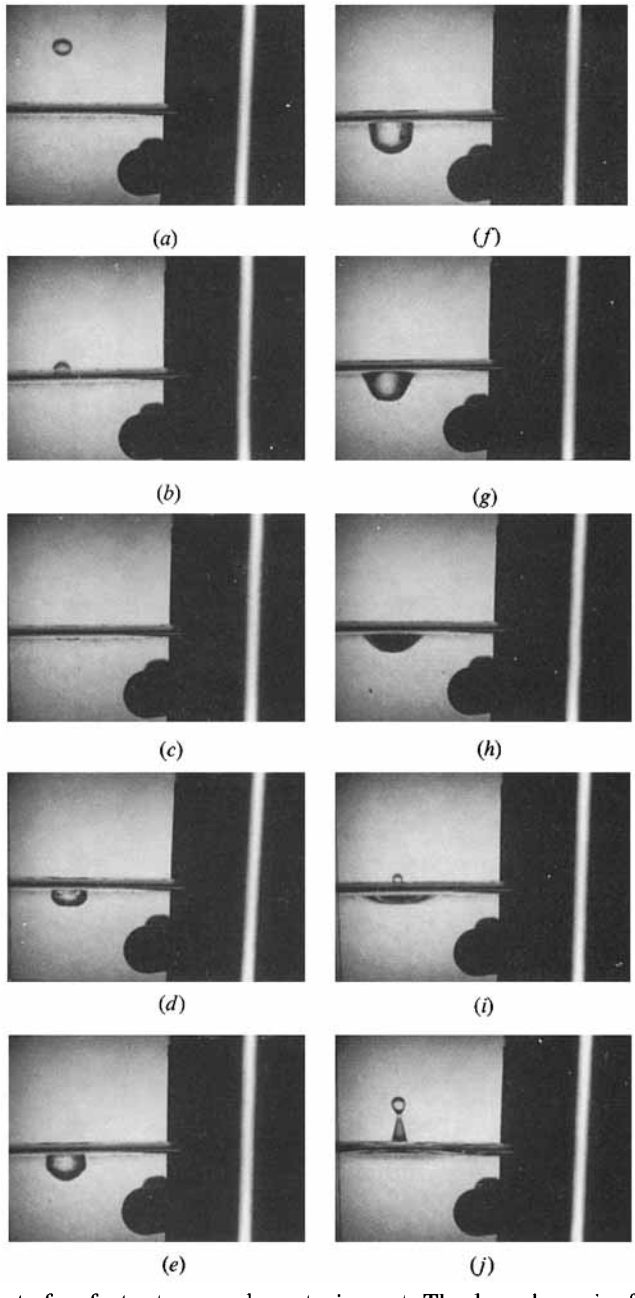

FIGURE 23. The effect of surfactant on regular entrainment. The drop shown is of a size and velocity for which regular entrainment should occur, as in figure 3. The addition of a surfactant (Kodak Photoflo) to the water suppresses the entrainment. (From Pumphrey 1989.)

5.2. *Rain noise in detail*

Use of a computer connected to a digital oscilloscope has enabled us to make repeated measurements of the frequencies, amplitudes and damping constants of the individual bubble pulses generated by the spray. We can use this information to find how the amplitude and damping vary, on average, as a function of frequency; the results are shown in figures 9 and 12 in the previous section. It is also possible to

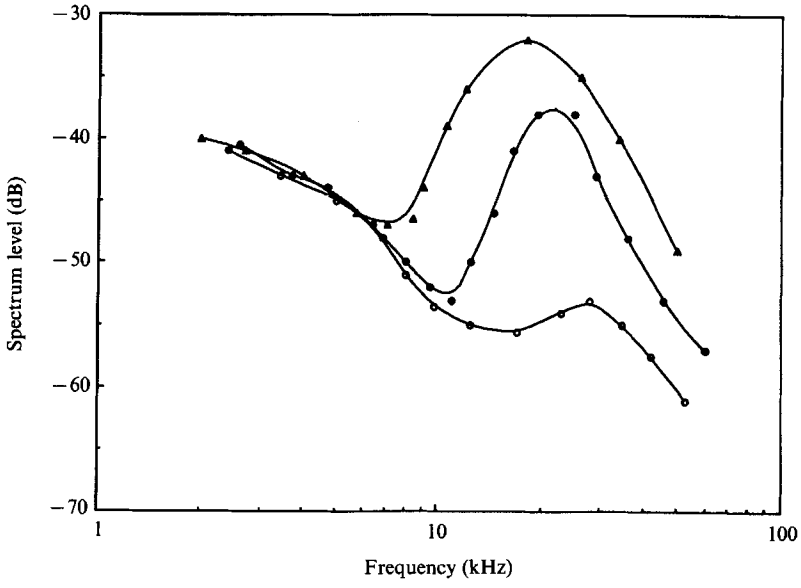

FIGURE 24. The effect of surfactant on the acoustic spectrum of the sound generated by a spray. The spectra shown are for clean water (triangles), low concentration of surfactant (filled circles) and high concentration (open circles). Note how the peak decreases in height and moves to a higher frequency as more surfactant is added.

measure the distribution of bubbles as a function of resonance frequency. We show typical results in figure 25; the distribution has the form $n(f) \propto 1/f^3$. If there are $n(f)$ bubbles entrained per second in a 1 Hz frequency band over a 1 m^2 area of the water surface, then it can be shown (Pumphrey & Crum 1990) that the intensity below the surface is given by

$$I_T = \frac{\pi n(f) D^2}{4\beta\rho c} = \frac{n(f) D^2 Q}{4f\rho c}, \tag{22}$$

and hence the intensity spectrum level is given by

$$\mathrm{ISL} = 10 \log \frac{\pi n(f) D^2/4\beta}{1\ \mu\mathrm{Pa}^2/\mathrm{Hz}} = 10 \log \frac{n(f) D^2 Q/4f}{1\ \mu\mathrm{Pa}^2/\mathrm{Hz}} \tag{23}$$

Note that Q decreases with increasing f, while D increases. These two effects partially cancel each other out, so the form of the spectrum is largely dominated by $n(f)$. We know the form of $n(f)$ from figure 25; we can calculate its absolute value if we know the total number of bubbles entrained per second over an area of 1 m^2. It can be seen from figure 16 that this is equal to the total number of drops with diameters between 0.8 and 1.1 mm which impact on that area per second. Scrimger *et al.* (1987) provide rain noise spectra and drop-size distributions which were measured simultaneously; we can therefore make a comparison between experimentally obtained spectra and those calculated from (23). The result is shown in figure 26, it can be seen that the shape of the spectrum is well predicted at frequencies above the peak frequency, but the absolute intensity is 4 dB higher than predicted. This is probably the result of several effects. One is that reverberations in the lake are making the sound louder than predicted; equation (23) is derived assuming water of infinite depth. Another possibility is that the instrument used to measure the raindrop size spectrum is not

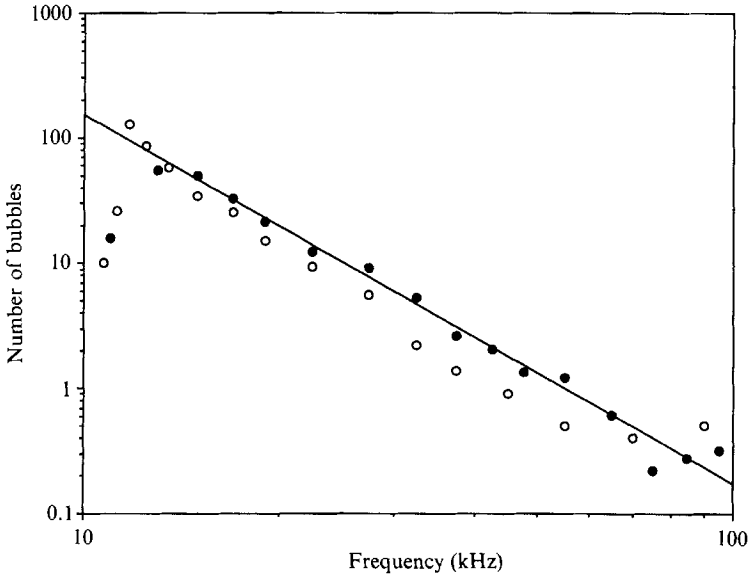

FIGURE 25. Number of bubbles entrained over a certain area of the water surface in an arbitrary time. The open circles are for bubbles entrained by real rain; the filled circles for bubbles entrained by artificial rain. The straight line is a power-law fit to the artificial rain data; the slope, i.e. the power, is -2.9.

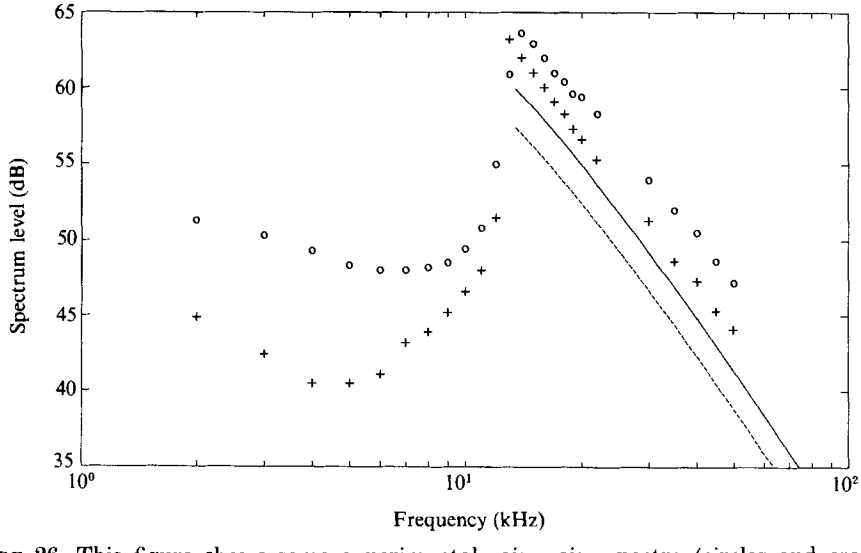

FIGURE 26. This figure shows some experimental rain noise spectra (circles and crosses) from Scrimger *et al.* (1987) and the predictions of equation (23) (solid and broken lines). The solid line corresponds to the circles; the broken line to the crosses. The predictions are 3 dB greater than those of Pumphrey & Crum (1990), this is apparently due to a numerical error in their calculations.

sensitive enough to very small drops and hence $n(f)$ is really rather larger than the data of Scrimger *et al.* suggest.

We can see from figure 16 that rain is not going to produce any sound at frequencies below 12–14 kHz by the regular entrainment mechanism. Real rain,

however, produces plenty of sound at frequencies below 12 kHz, so there must be some other process occurring. This is either irregular entrainment, or the initial impact sound, it has not yet been determined which of these two effects is the most important. It is known, however, that the initial impact sound consists of a very narrow spike, with a width of less than 10 μs and hence might be expected to have a rather flat spectrum at frequencies below 100 kHz. Irregular entrainment, on the other hand, produces many bubbles with resonance frequencies in the 1–10 kHz range, so it seems likely that it is this process which causes the low-frequency part of the rain noise spectrum.

6. Large bubble entrainment

This is a process that occurs in a rather small range of d and v, approximately where regular entrainment ceases because the drop is too large, as shown in figure 5. Figure 27 shows a series of frames from a high-speed movie of the process. The bubble entrained is rather large, in this case it has a measured diameter of 4.6 ± 0.2 mm, for which (10) predicts a resonance frequency of 1.00 ± 0.06 kHz. The measured value is 1.3 kHz; the 30% increase may be attributed to a combination of the bubble's non-sphericity and its proximity to a free surface (Strasberg 1953). Note also that this process is fundamentally different from that observed by Franz and by Engel at very large impact energies, even though both processes result in a large bubble floating at the surface. There, the crown or film rises vertically and joins at the top to form a floating bubble, while here, the base of the cavity appears to spread out into a dish-shape which then detaches from the cavity to form a very distorted bubble, at a depth of one or two bubble radii below the surface. The bubble then floats up to the surface some 100 ms later. This process is included for completeness, it is unlikely to be very important in nature as it only occurs in a small area of the (d, v)-plane. It is possible that this process, unlike regular entrainment, is partly caused by shape oscillations of the drop as it falls.

7. Mesler entrainment

We now describe yet another sort of bubble entrainment which we shall refer to as Mesler entrainment, after a scientist who studied it extensively (Esmailizadeh & Mesler 1986; Carrol & Mesler 1981), but was apparently unaware of the various other processes described above. It is characterized by the entrainment of many bubbles by one drop impact; these bubbles are very small (50 μm is typical) and they emit very little noise, which is presumably why they have been overlooked or ignored by the acoustics community. This type of entrainment seems to occur most often for very small impact velocities, below the regular entrainment region, but may occasionally occur in conjunction with irregular entrainment, at the collapse of the water column. It is very unpredictable; the number of bubbles entrained varies greatly from one drop to the next, even if the drops are of the same size and impact velocity. It is also extremely sensitive to the cleanness of the water. It is very difficult to photograph Mesler entrainment as it actually occurs so it is as yet unclear how the process works; it does seem, however, to take place in the very early stages of the impact. A plausible mechanism has been proposed by Oguz & Prosperetti (1989); their description is roughly as follows. As the point of contact between drop and surface spreads, a capillary wave is formed which travels outward from the point of contact, on both the drop and the surface. Because the drop is moving downwards,

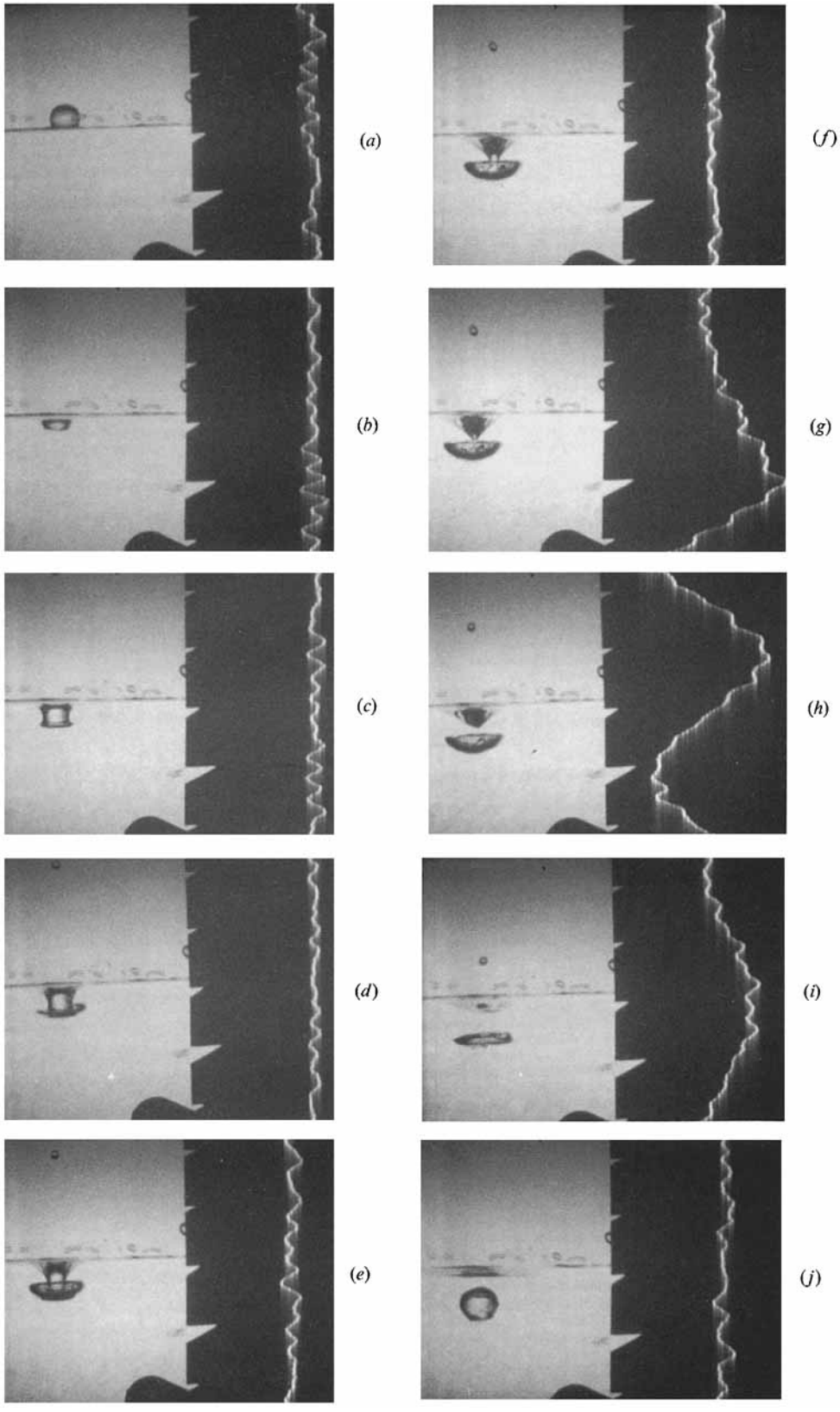
(a)
(b)
(c)
(d)
(e)
(f)
(g)
(h)
(i)
(j)

FIGURE 28. Mesler entrainment, as caused by a drop of approximately 5 mm diameter impacting at a speed of about 0.5 m/s. The photograph was taken by one of the authors (H.C.P.) using time-delayed flash photography; the equipment used is described in Pumphrey & Walton (1988).

the wave crests on the drop and on the surface meet, thereby trapping a very thin toroidal, or ring-shaped bubble. This is very unstable and breaks very rapidly into a ring of tiny spherical bubbles. The process may be repeated several times, giving several such rings of bubbles. One can obtain pictures of the beautiful patterns made by the bubbles as they are swirled around by the flow which results from the impact. Frequently, a vortex ring is formed, which can sweep bubbles down to a great depth. Figure 28 shows a typical example; for others see Esmailizadeh & Mesler (1986) and Carrol & Mesler (1981).

8. Conclusions

Various phenomena have been described in which the impact of a water drop on a water surface causes the entrainment of one or more bubbles. These phenomena occur for different ranges of the parameters d, the drop diameter and v, the impact velocity. Figure 5 is an attempt to show in one figure the areas of the (d, v)-plane in which all of the above processes occur. The accuracy with which these regions are defined is extremely variable; the regular entrainment region is very accurately known, while irregular entrainment can occur anywhere above this in the diagram. The region actually marked for irregular entrainment is where the splash is so

FIGURE 27. Large bubble entrainment. This sequence shows a drop of 5.8 ± 0.1 mm diameter impacting at a speed of 1.0 ± 0.1 m/s. Note the bubble detaches and the sound begins in frame (*g*). The sound is a damped sinewave, it does not look like one because it is of such a low frequency that there is less than one cycle in each frame. The high-frequency noise on the oscilloscope trace is caused by the camera. The times in ms of each frame after the drop impact are: (*a*) 0, (*b*) 7, (*c*) 10, (*d*) 12, (*e*) 15, (*f*) 19, (*g*) 20, (*h*) 21, (*i*) 29, (*j*) 62.

energetic that bubbles are nearly always entrained. Mesler entrainment can occur anywhere, but is most noticeable in the region marked because no other process occurs here.

So far, the main practical use of this material is to explain the underwater sound produced by rain, which is of interest for remote weather sensing. There may be other applications, for example, Mesler entrainment was originally studied in an attempt to understand some phenomena that occur when water boils.

This work was supported by the Office of Naval Research and the Johns Hopkins University.

REFERENCES

CARROL, K. & MESLER, R. 1981 Bubble nucleation studies. Part II: Bubble entrainment by drop-formed vortex rings. *AIChE J.* **27**, 853–856.

CHAPMAN, D. S. & CRITCHLOW, P. R. 1967 Formation of vortex rings from falling drops. *J. Fluid Mech.* **29**, 177–185.

CROWTHER, P. 1988 Bubble noise creation mechanisms. In *Sea Surface Sound* (ed. B. R. Kerman) pp. 131–150. Kluwer.

DEVIN, C. 1959 Survey of thermal, radiation, and viscous damping of pulsating air bubbles in water. *J. Acoust. Soc. Am.* **31**, 1654–1667.

DINGLE, A. N. & LEE, Y. 1972 Terminal fallspeeds of raindrops. *J. Appl. Met.* **11**, 877–879.

ELMORE, P., PUMPHREY, H. C. & CRUM, L. A. 1989 Further studies of the underwater noise produced by rainfall. *National Center for Physical Acoustics Tech. Rep.* NCPA LC.02.89.

ENGEL, O. G. 1966 Crater depth in fluid impacts. *J. Appl. Phys.* **37**, 1798–1808.

ESMAILIZADEH, L. & MESLER, R. 1986 Bubble entrainment with drops. *J. Colloid Interface Sci.* **110**, 561–574.

FRANZ, G. J. 1959 Splashes as sources of sound in liquids. *J. Acoust. Soc. Am.* **31**, 1080–1096.

GUNN, R. & KINZER, G. D. 1949 The terminal velocity of fall for water droplets in stagnant air. *J. Met.* **6**, 243–248.

HARLOW, F. H. & SHANNON, J. P. 1967 The splash of a liquid drop. *J. Appl. Phys.* **38**, 3855–3866.

LAWS, J. O. 1941 Measurements of the fall velocity of water-drops and raindrops. *Trans. Am. Geophys. Un., Hydrology papers* **22**, 709–721.

LONGUET-HIGGINS, M. S. 1989*a* Monopole emission of sound by asymmetric bubble oscillations. Part 1. Normal modes. *J. Fluid Mech.* **201**, 525–541.

LONGUET-HIGGINS, M. S. 1989*b* Monopole emission of sound by asymmetric bubble oscillations. Part 2. An initial value problem. *J. Fluid Mech.* **201**, 543–565.

LONGUET-HIGGINS, M. S. 1990 An analytic model of sound production by raindrops. *J. Fluid Mech.* **214**, 395–410.

MINNAERT, M. 1933 On musical air-bubbles and the sounds of running water. *Phil. Mag.* **16**, 235–248.

NYSTUEN, J. A. 1986 Rainfall measurements using underwater ambient noise. *J. Acoust. Soc. Am.* **79**, 972–982.

OGUZ, H. N. & PROSPERETTI, A. 1989 Surface tension effects in the contact of liquid surfaces. *J. Fluid Mech.* **203**, 149–171.

OGUZ, H. N. & PROSPERETTI, A. 1990*a* Bubble entrainment by the impact of drops on liquid surfaces. *J. Fluid Mech.* **219**, 143–179.

OGUZ, H. N. & PROSPERETTI, A. 1990*b* The underwater noise of rain. *J. Fluid Mech.* (submitted).

PROSPERETTI, A. 1988 Bubble dynamics in oceanic ambient noise. In *Sea Surface Sound* (ed. B. R. Kerman) pp. 151–172. Kluwer.

PUMPHREY, H. C. 1989 Sources of ambient noise in the ocean: an experimental investigation. Ph.D. dissertation, University of Mississippi.

PUMPHREY, H. C. & CRUM, L. A. 1990 Free oscillations of near-surface bubbles as a source of the underwater noise of rain. *J. Acoust. Soc. Am.* **87**, 142–148.

PUMPHREY, H. C., CRUM, L. A. & BJØRNØ, L. 1989 Underwater sound produced by individual drop impacts and rainfall. *J. Acoust. Soc. Am.* **85**, 1518–1526.

PUMPHREY, H. C. & WALTON, A. J. 1988 Experimental study of the sound emitted by water drops impacting on a water surface. *European J. Phys.* **9**, 225–231.

RAYLEIGH, LORD 1890 On the tension of recently formed liquid surfaces. *Proc. R. Soc. Lond.* **47**, 281–287.

SCRIMGER, J. A. 1985 Underwater noise caused by precipitation. *Nature* **318**, 647–649.

SCRIMGER, J. A., EVANS, D. J., MCBEAN, G. A., FARMER, D. M. & KERMAN, B. R. 1987 Underwater noise due to rain, hail and snow. *J. Acoust. Soc. Am.* **81**, 79–86.

SCRIMGER, J. A., EVANS, D. J. & YEE, W. 1989 Underwater noise due to rain – open ocean measurements. *J. Acoust. Soc. Am.* **85**, 726–731.

STRASBERG, M. 1953 The pulsation frequency of non-spherical gas bubbles in liquids. *J. Acoust. Soc. Am.* **25**, 536–537.

STRASBERG, M. 1956 Gas bubbles as sources of sound in liquids. *J. Acoust. Soc. Am.* **28**, 20–26.

WORTHINGTON, A. M. 1908 *A Study of Splashes.* Longmans, Green and Co.